J. Fluid Mech. (2007), *vol.* 572, *pp.* 179–188. © 2007 Cambridge University Press
doi:10.1017/S0022112006003673 Printed in the United Kingdom

Numerical study of turbulent magnetohydrodynamic channel flow

By THOMAS BOECK[1], DMITRY KRASNOV[1] AND EGBERT ZIENICKE[2]

[1]Fakultät Maschinenbau, Technische Universität Ilmenau, Postfach 100565, 98684 Ilmenau, Germany
[2]Institut für Physik, Technische Universität Ilmenau, Postfach 100565, 98684 Ilmenau, Germany

(Received 22 December 2005 and in revised form 9 October 2006)

Mean flow properties of turbulent magnetohydrodynamic channel flow with electrically insulating channel walls are studied using high-resolution direct numerical simulations. The Lorentz force due to the homogeneous wall-normal magnetic field is computed in the quasi-static approximation. For strong magnetic fields, the mean velocity profile shows a clear three-layer structure consisting of a viscous region near each wall and a plateau in the middle connected by logarithmic layers. This structure reflects the significance of viscous, turbulent, and electromagnetic stresses in the streamwise momentum balance dominating the viscous, logarithmic, and plateau regions, respectively. The width of the logarithmic layers changes with the ratio of Reynolds- and Hartmann numbers. Turbulent stresses typically decay more rapidly away from the walls than predicted by mixing-length models.

1. Introduction

Turbulent magnetohydrodynamic (MHD) flows at low magnetic Reynolds numbers occur in a variety of metallurgical processes (Davidson 1999; Moreau 2003) such as the electromagnetic braking of molten steel in continuous casting and in electromagnetic stirring of melts. They may also occur in liquid-metal cooling blankets for the toroidal plasma chamber in present and future fusion reactor designs.

By comparison with ordinary fluid flows, the experimental investigation of MHD flows is complicated by the opacity and corrosiveness of liquid metals. Experiments typically provide very limited information on the flow structures and statistics. Reliable numerical simulations should therefore be even more of a necessity for turbulent MHD flows than in ordinary hydrodynamics. However, many MHD flow computations are performed using the Reynolds-averaged Navier–Stokes (RANS) equations with standard turbulence models and wall functions. There are current efforts to improve on this *ad hoc* approach through the development of MHD-specific turbulence models (Kenjereš & Hanjalić 2000; Widlund, Zahrai & Bark 1998) and wall functions, both for RANS and large-eddy simulations (LES).

Direct numerical simulations (DNS) are valuable to this effort as a database for model calibration. They are also important for studying fundamental aspects of turbulent MHD flows such as anisotropy at large and small length scales or Joule dissipation. DNS have been performed in periodic domains, i.e. without wall effects (Zikanov & Thess 1998; Knaepen, Kassinos & Carati 2004). By contrast, DNS of wall-bounded turbulent MHD flows (Lee & Choi 2001; Satake *et al.* 2005) have been fewer and less systematic. Recent LES of turbulent Hartmann flow by Kobayashi

https://doi.org/10.1017/S0022112006003673 Published online by Cambridge University Press

(2006), i.e. of channel flow with a homogeneous wall-normal magnetic field, have examined the performance of certain subgrid-stress models but were only compared with experimental measurements of limited accuracy. Our present work, in which we report a series of DNS of turbulent Hartmann flow, should therefore be of interest for those involved in LES and RANS modelling for MHD flows.

Experimental and theoretical work on Hartmann flow goes back to Hartmann (1937). In the laminar case the bulk velocity is uniform because of the balance of Lorentz force and pressure gradient. Viscous effects are confined to the so-called Hartmann layers near the channel walls. The size of these layers is inversely proportional to the magnetic field strength, which is measured by the dimensionless Hartmann number.

Hartmann & Lazarus (1937) took measurements of the pressure loss for laminar and turbulent Hartmann flows. Later experiments, in particular by Branover, Lykoudis, and their coworkers, have also provided measurements of velocity profiles and turbulent stresses but could not resolve well the near-wall regions. The book by Branover (1978) summarizes these works. At the same time, turbulence models based on the mixing-length hypothesis were proposed by various authors. Some of these models account for the damping of the turbulent stress due to the Lorentz force through suitable prefactors in the mixing-length ansatz. The adjustable parameters are then fitted to measurements of pressure loss in the experiments. An exemplary work is that by Lykoudis & Brouillette (1967), who formulated their own model and performed experiments as well. Recently, Alboussière & Lingwood (2000) have revisited this problem and formulated a mixing-length model without heuristic MHD corrections to the ansatz for the turbulent stresses from ordinary turbulent shear flow.

Further recent works have focused on the problem of transition to turbulence in Hartmann flow. As in other shear flows, ordinary linear stability theory provides an instability threshold far beyond the practically observed limits. Moresco & Alboussière (2004) performed an experiment in an annular duct and detected transition at variance with earlier experiments on re-laminarization but in agreement with our own numerical studies (Krasnov *et al.* 2004; Zienicke & Krasnov 2005), in which a two-step transition scenario is assumed. It is based on transient amplification of streamwise-independent vortices in the laminar Hartmann layers, which subsequently become unstable to three-dimensional noise. The present paper arises from a continuation of our transition simulations into the turbulent parameter range.

The goal of the DNS reported in this paper is to obtain developed turbulent states for different Reynolds and Hartmann numbers. For these turbulent states we systematically examine the structure of mean profiles and their parameter dependence. In particular, we approach the case of an isolated, turbulent Hartmann layer by increasing the Hartmann number Ha for fixed ratios of Reynolds and Hartmann numbers. Comparison with other works will be made through the solution of the mixing-length turbulence models by Lykoudis & Brouillette (1967) suitable for interacting turbulent Hartmann layers, and of the recent model by Alboussière & Lingwood (2000) for an isolated turbulent Hartmann layer. We shall also assess the criterion for the non-overlap of turbulent Hartmann layers proposed in Harris (1960) and later in Alboussière & Lingwood (2000) based on our simulation results.

2. Parameter definition and simulation procedure

Our numerical study of turbulent Hartmann flow is based on the quasi-static approximation of liquid-metal MHD (Branover 1978). This approximation has been

https://doi.org/10.1017/S0022112006003673 Published online by Cambridge University Press

R	Ha	L_x	L_y	$N_x \times N_y \times N_z$	R_{av}	Re_τ	c_f	T_a
450	10	5π	2π	$256 \times 256 \times 128$	4.05×10^2	240.7	7.06×10^{-3}	223
450	15	$\frac{10}{3}\pi$	$\frac{4}{3}\pi$	$256 \times 256 \times 256$	4.20×10^2	359.2	6.50×10^{-3}	212
450	20	3π	$\frac{6}{5}\pi$	$256 \times 256 \times 256$	4.27×10^2	475.8	6.21×10^{-3}	128
450	30	$\frac{10}{3}\pi$	$\frac{16}{15}\pi$	$256 \times 256 \times 256$	4.35×10^2	710.8	5.93×10^{-3}	207
500	10	4π	2π	$256 \times 256 \times 128$	4.5×10^2	268.2	7.11×10^{-3}	300
500	15	$\frac{10}{3}\pi$	$\frac{4}{3}\pi$	$256 \times 256 \times 256$	4.667×10^2	398.8	6.49×10^{-3}	240
500	20	$\frac{8}{3}\pi$	$\frac{16}{15}\pi$	$256 \times 256 \times 256$	4.75×10^2	528.4	6.18×10^{-3}	114
500	30	2π	$\frac{4}{5}\pi$	$256 \times 256 \times 256$	4.833×10^2	785.9	5.87×10^{-3}	92
700	10	$\frac{10}{3}\pi$	$\frac{4}{3}\pi$	$256 \times 256 \times 128$	6.30055×10^2	365.0	6.72×10^{-3}	328
700	15	$\frac{8}{3}\pi$	$\frac{16}{15}\pi$	$256 \times 256 \times 256$	6.5333×10^2	538.0	6.02×10^{-3}	84
700	20	2π	$\frac{4}{5}\pi$	$256 \times 256 \times 256$	6.65×10^2	708.6	5.67×10^{-3}	116
700	30	2π	$\frac{4}{5}\pi$	$512 \times 512 \times 256$	6.76×10^2	1047.3	5.33×10^{-3}	58
900	10	3π	$\frac{6}{5}\pi$	$256 \times 256 \times 256$	8.101×10^2	456.0	6.34×10^{-3}	165
900	15	$\frac{12}{5}\pi$	π	$256 \times 256 \times 256$	8.40×10^2	681.3	5.84×10^{-3}	183
900	20	2π	$\frac{4}{5}\pi$	$512 \times 256 \times 256$	8.55×10^2	891.9	5.44×10^{-3}	82
900	25	2π	$\frac{4}{5}\pi$	$512 \times 512 \times 256$	8.64×10^2	1101.0	5.20×10^{-3}	51

TABLE 1. Simulation parameters and results. N_x, N_y and N_z denote the number of collocation points with respect to the coordinates x, y and z. The time interval T_a is the averaging time in convective units d/U_0.

validated by Lee & Choi (2001) through comparison with the full MHD equations. Our pseudospectral numerical code is based on a Fourier–Chebyshev expansion. The equations and boundary conditions as well as details of the numerical method can be found in Krasnov *et al.* (2004). Since then, the code has been improved by implementing a second-order-accurate time-stepping method and de-aliasing. We choose the coordinate system such that the channel walls coincide with planes $z = \mathrm{const}$. The streamwise coordinate is x, and the wall-normal coordinate is z. The Hartmann number Ha and the Hartmann layer thickness δ are defined by

$$Ha = \frac{d}{\delta}, \quad \delta = \frac{1}{B_0}\sqrt{\frac{\rho\nu}{\sigma}}, \tag{2.1}$$

where B_0 is the applied magnetic field and d denotes the half-channel width. The other symbols are the electric conductivity σ, the density ρ and kinematic viscosity ν of the liquid. In the simulations, the volume flux Q per span-width in the streamwise direction, and thereby the average streamwise velocity U_{av}, are prescribed. For a given Hartmann number, U_{av} and the laminar centreline velocity U_0 are related by $U_{\mathrm{av}} \approx U_0\,(1 - 1/Ha)$ for $Ha > 5$. This relation is found by integrating the laminar velocity profile (Branover 1978). As in our work on transition (Krasnov *et al.* 2004) we shall prescribe the Reynolds number $R = U_0\delta/\nu$ based on the Hartmann layer thickness and U_0. The Reynolds number R_{av} is based on U_{av} instead of U_0. Likewise, one can define two different global Reynolds numbers, namely $Re = HaR$ and $Re_{\mathrm{av}} = HaR_{\mathrm{av}}$ based on the half-channel width d and U_0 and U_{av}, respectively. Table 1 lists the parameter

https://doi.org/10.1017/S0022112006003673 Published online by Cambridge University Press

combinations for R and Ha in our simulations as well as the dimensions L_x and L_y of the computational domain (in units of d). It also contains the friction coefficient $c_f = 2\tau_w/\rho U_{\mathrm{av}}^2$ and the friction Reynolds number $Re_\tau = u_\tau d/\nu$, which are simulation results. The friction velocity u_τ is defined with the average wall shear stress $\tau_w = \rho u_\tau^2$.

In the simulations, the dimensions L_x and L_y had to be large enough to obtain a turbulent state without long-range spatial correlations on the scale of L_x and L_y. At the same time, they had to be chosen as small as possible in order to keep the resolution requirements and the necessary amount of computer time manageable. We have therefore reduced L_x and L_y as Re_τ increased when moving to higher Ha at fixed R (as can be seen in the snapshots of figure 1). Reduction of L_x and L_y with increasing Re_τ is also used in ordinary channel turbulence (Moser, Kim & Mansour 1999). We have checked that two-point correlations in the streamwise and spanwise coordinates are essentially zero at maximum separation (half the lateral domain size) for a fixed position $z = 1/Ha$. The number of modes was large enough to ensure that energy spectra show significant decay at high wavenumbers.

The simulations were typically started with initial data from a completed simulation with similar value of Re_{av}. Averaging of the flow quantities was started only after the transition to the new statistically stationary state had been completed. For this purpose we have monitored the transients in global quantities such as the total kinetic energy of the flow. The averaging time T_a was on the order of $100d/U_0$. Each of the runs in table 1 therefore represents a substantial computation. The simulations were mostly performed on cluster computers with Pentium 4 or Opteron processors. The typical mono-processor time for a simulation with $N_x = N_y = N_z = 256$ was about 4000 hours. The case $R = 900$ and $Ha = 25$ took about 12000 hours.

3. Mean flow properties

Figure 1 illustrates how the streamwise velocity distribution develops a plateau upon increasing the magnetic field strength while R is kept constant. The turbulence is increasingly confined near the walls but develops smaller scales thanks to the increase in Re_τ. The case with the relatively small value $Ha = 10$ in figure 1(b) appears rather similar to ordinary hydrodynamics shown in figure 1(a).

The mean flow properties of Hartmann flow are governed by the Reynolds equation

$$\rho\nu\frac{\partial^2 u}{\partial z^2} + \frac{\partial \tau_T}{\partial z} - \sigma B_0^2 (u - U_{\mathrm{av}}) - \frac{\partial p}{\partial x} = 0, \tag{3.1}$$

where $u(z)$ is the averaged streamwise velocity and $\tau_T(z) = -\rho\langle u'w'\rangle$ is the turbulent stress caused by the fluctuating streamwise and wall-normal velocity components u' and w'. The Lorentz force is given by $-\sigma B_0^2 (u - U_{\mathrm{av}})$. One can write (3.1) as $\mathrm{d}\tau/\mathrm{d}z = \partial p/\partial x$, where τ is the sum of the viscous stress $\tau_v = \rho\nu \mathrm{d}u/\mathrm{d}z$, the turbulent stress τ_T and the electromagnetic stress τ_m representing the integrated Lorentz force term in (3.1). As in ordinary channel flow, the total stress τ is an antisymmetric linear function with respect to the middle of the channel.

The non-dimensional form of (3.1) based on u_τ and the length scale ν/u_τ was derived in Lykoudis & Brouillette (1967). It is

$$\frac{\mathrm{d}^2 u}{\mathrm{d}z^2} + \frac{\mathrm{d}\tau_T}{\mathrm{d}z} - \frac{2}{R_{\mathrm{av}}^2 c_f}(u - \sqrt{2/c_f}) + \frac{1}{R_{\mathrm{av}} Ha}\sqrt{\frac{2}{c_f}} = 0. \tag{3.2}$$

https://doi.org/10.1017/S0022112006003673 Published online by Cambridge University Press

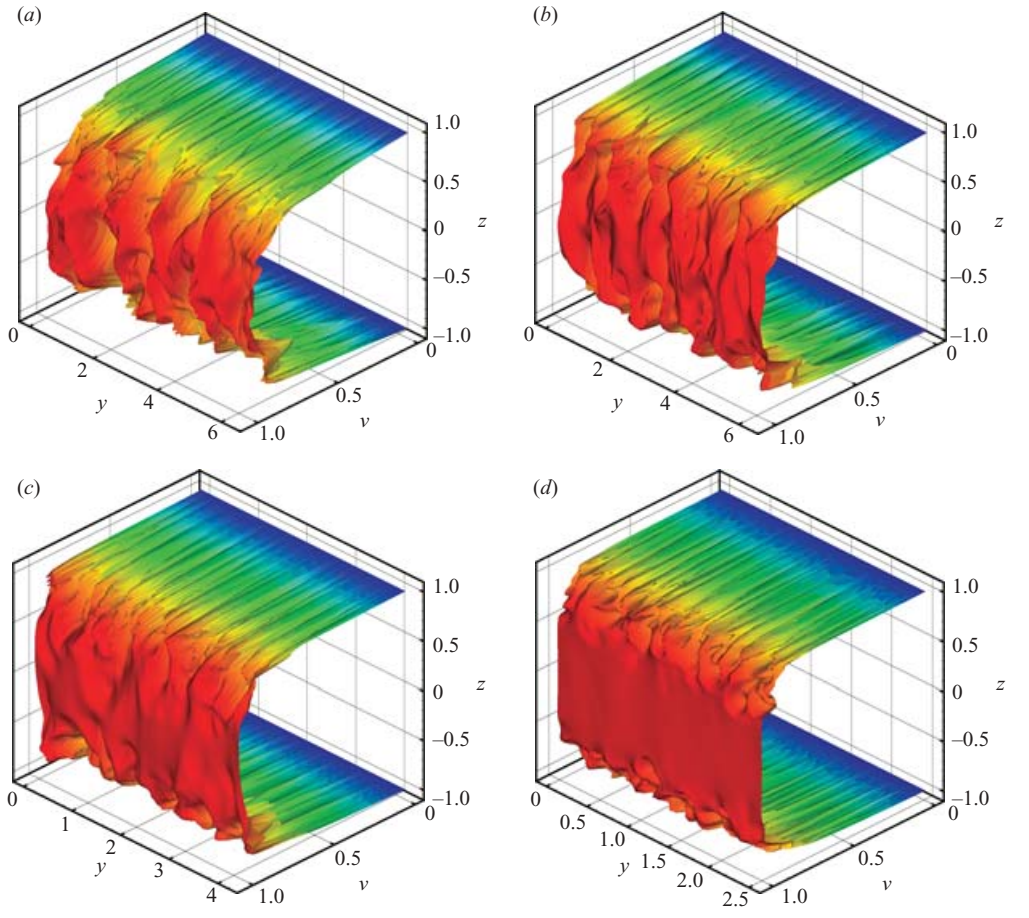


FIGURE 1. Snapshots of the streamwise velocity component in a plane $x = \text{const}$. Non-magnetic flow at $Re = 3300$ (a) and turbulent Hartmann flow at $R = 500$ and $Ha = 10$ (b), $Ha = 15$ (c) and $Ha = 30$ (d).

It is customary to write the non-dimensional quantities with a superscript $+$, which we omit for simplicity in (3.2).

Profiles of the mean streamwise velocity component are shown in figure 2. We can identify three different regions in the profiles in figure 2(a–c). The viscous sublayer (with $u^+ \sim z^+$) marked as region I is followed by a logarithmic layer (with $u^+ \sim A \log(z^+) + B$) marked as region II, which starts around $z^+ \sim 30 \ldots 40$. A plateau region marked III is formed at sufficiently large Ha. The profiles for different Ha then essentially coincide except for the width of the plateau. This can be seen clearly at $R = 450$ and $R = 500$, where the logarithmic range is rather short. Notice that we have drawn the mean velocity profiles for the entire channel in these plots to highlight the plateau region and to distinguish the different values of Ha by the falling flanks of the profiles. On physical grounds they should only have been drawn up to the middle of the channel.

Figure 2(a–c) also shows that the logarithmic range becomes wider as R increases. Figure 2(d) compares the profiles at the highest Ha for each R. We see clearly how the plateau shrinks upon increasing R for $Ha = 30$. For $R = 900$ we have only managed a simulation for $Ha = 25$, where a plateau is barely present. From $R = 450$

https://doi.org/10.1017/S0022112006003673 Published online by Cambridge University Press

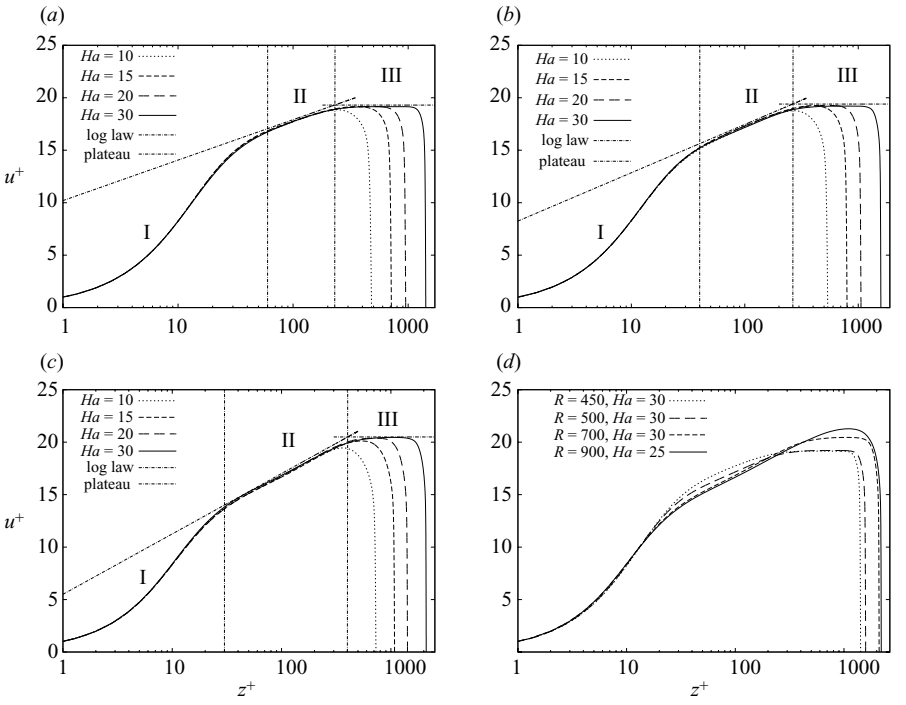


FIGURE 2. Semi-logarithmic plots of mean velocity profiles for $R = 450$ (a), $R = 500$ (b) and $R = 700$ (c), in units based on the friction velocity u_τ. (d) The profiles at the highest Ha for each R. The logarithmic law drawn in (a) and (b) is somewhat arbitrary.

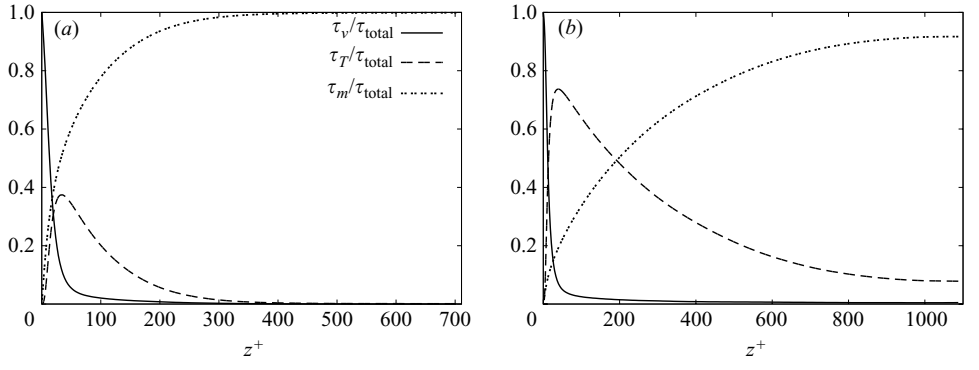


FIGURE 3. Stress distributions from DNS: fractions of the viscous, turbulent and electromagnetic stress for $R = 450$, $Ha = 30$ (a) and $R = 900$, $Ha = 25$ (b).

to $R = 700$ the slope A increases whereas the offset B is decreases. The difference between $R = 700$ and $R = 900$ in the logarithmic range is only slight. At $R = 900$ and $Ha = 25$ the values $A = 2.4$ and $B = 5.65$ provide a good fit.

The increasing width of the logarithmic layer with R is related to larger contributions of the turbulent stress to the total stress. Figure 3 shows the relative size of the viscous, turbulent and electromagnetic stress terms as functions of the wall distance. For $R = 450$ and $Ha = 30$ the turbulent stress contributes less than half of the total stress over a short range only. By contrast, it is dominant over a significant range for $R = 900$.

https://doi.org/10.1017/S0022112006003673 Published online by Cambridge University Press

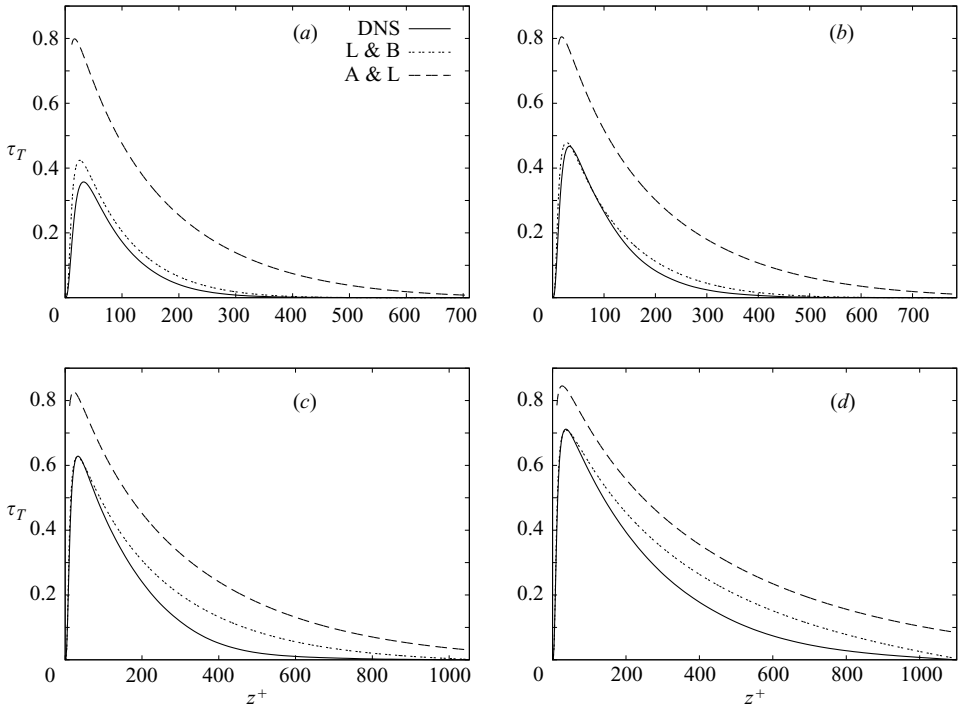


FIGURE 4. Turbulent stress distributions from DNS (bold line) and from models of Lykoudis & Brouillette (L & B) (dot-dotted) and Alboussière & Lingwood (A & L) (dashed). Flow regimes are $R=450$, $Ha=30$ (*a*), $R=500$, $Ha=30$ (*b*), $R=700$, $Ha=30$ (*c*) and $R=900$, $Ha=25$ (*d*). The A & L model assumes $Ha\to\infty$ and is limited to $z^+>11.3$.

The models by Lykoudis & Brouillette (1967) and Alboussière & Lingwood (2000) for the turbulent stress τ_T in (3.2) are based on the mixing-length ansatz with certain additional corrections. Lykoudis & Brouillette (1967) propose

$$\tau_T=\gamma_1(z)\,\gamma_2(z,c_f,R)\,\gamma_3(c_f,R)\,\kappa^2\left(z\frac{\mathrm{d}u}{\mathrm{d}z}\right)^2 \tag{3.3}$$

with the van Driest correction γ_1 to suppress the turbulent stress near the wall. The factor γ_2 is introduced to account for the magnetic damping of vortices perpendicular to the magnetic field, and the additional coefficient γ_3 describes the magnetic damping of turbulence away from the wall. The von Kármán constant is $\kappa=0.4$.

Equation (3.2) with this ansatz amounts to a nonlinear eigenvalue problem for c_f. The three boundary conditions are $u=0$, $\mathrm{d}u/\mathrm{d}z=1$ at $z=0$ and $\mathrm{d}u/\mathrm{d}z=0$ in the middle of the channel located at $z_m=Re_{\mathrm{av}}\sqrt{c_f/2}$.

The model of Alboussière & Lingwood (2000) applies in the limit $Ha\to\infty$ in (3.2), whereby the pressure term drops out and $z_m\to\infty$. The correction terms γ_i of Lykoudis & Brouillette (1967) are discarded, and the viscous sublayer is introduced by setting the sum of viscous and turbulent stresses equal to the wall stress at $z^+=11.3$. Another change is to treat the sum of viscous and turbulent stresses as being represented by the mixing-length ansatz (3.3).

Figure 4 shows that the peak values of the distributions of τ_T are captured well by the model of Lykoudis & Brouillette (1967), in contrast to the model of Alboussière & Lingwood (2000). The decay of τ_T is more rapid than predicted by

https://doi.org/10.1017/S0022112006003673 Published online by Cambridge University Press

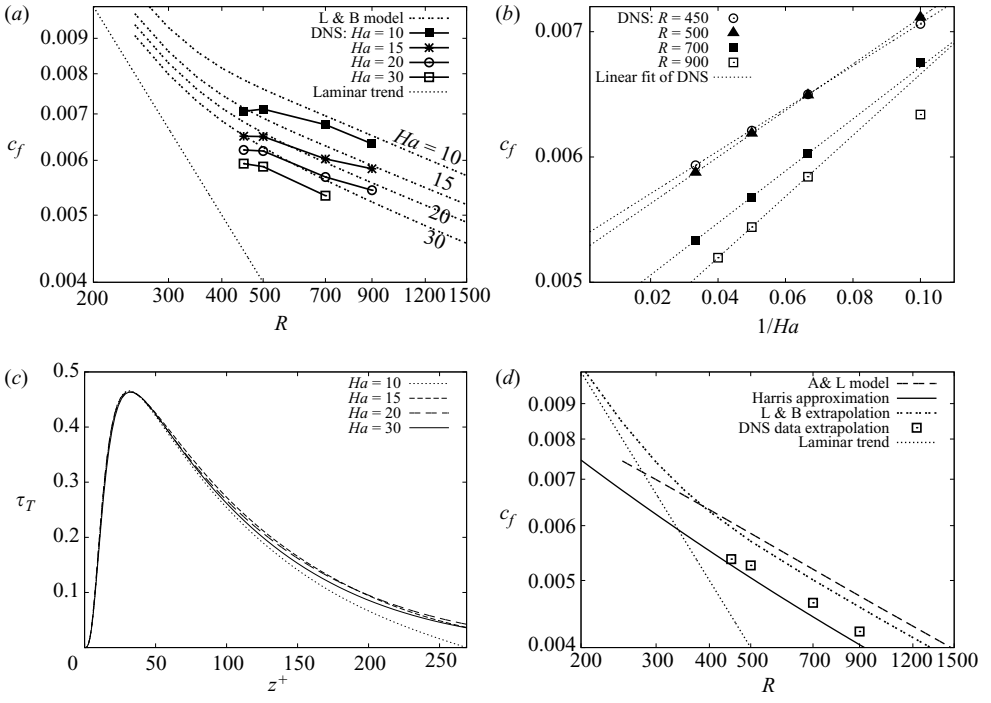


FIGURE 5. c_f vs. R (a) and vs. $1/Ha$ (b). (c) Turbulent stresses for $R = 500$ from DNS and (d) c_f vs. R from models and DNS for $Ha \to \infty$. The laminar result $c_f = 2/R$ for infinite Ha is shown for comparison in (a, d), which are in logarithmic scale.

the models, with particularly large differences for the higher values of R. Concerning the apparently good agreement between our results and the model of Lykoudis & Brouillette (1967) one should also bear in mind that the friction Reynolds numbers are up to 5% larger for the model, i.e. the positions of the peaks would be somewhat shifted when the results are plotted in units of the half-channel width d and centreline velocity U_0.

4. Friction coefficient

The dependence of the friction coefficient c_f on R from the DNS and from the model of Lykoudis & Brouillette (1967) is shown in figure 5(a). The differences are significant for low R, where the DNS results show a local maximum at $R = 500$ for $Ha = 10$ and $Ha = 15$, in contrast to the model. This behaviour suggests proximity of the transition threshold, which has been detected at $R \approx 400$ in Krasnov *et al.* (2004).

The dependence of c_f on Ha at fixed R is shown in figure 5(b). We plot c_f vs. $1/Ha$ because the model of Lykoudis & Brouillette (1967) satisfies the asymptotic relation

$$c_f \sim c_f^{(0)}(R_{\mathrm{av}}) + \frac{1}{Ha} c_f^{(1)}(R_{\mathrm{av}}) \tag{4.1}$$

for $1/Ha \to 0$. Assuming that the expansion coefficients of c_f in (4.1) are continuously differentiable functions of R_{av}, it is clear that dependence of c_f on $1/Ha$ for fixed R instead of fixed R_{av} is also linear for $Ha \to \infty$ because $R_{\mathrm{av}} \sim R(1 - 1/Ha)$ (for $Ha > 5$). We see that the DNS results lie on straight lines in figure 5(b) except for the

https://doi.org/10.1017/S0022112006003673 Published online by Cambridge University Press

lowest values of Ha for $R = 700$ and $R = 900$. We can therefore extrapolate our DNS results to the limit $Ha \to \infty$.

The asymptotic relation (4.1) can be justified from (3.2), in which the pressure term is a linear perturbation term in $1/Ha$ (provided that the boundary condition $\mathrm{d}u/\mathrm{d}z = 0$ applies effectively at $z_m \to \infty$). The other terms in (3.2) are independent of Ha, in particular the turbulent stress term proposed by Lykoudis & Brouillette (1967). Figure 5(*c*) demonstrates that the turbulent stress becomes independent of Ha in our DNS when Ha is sufficiently large, which supports the asymptotic linear dependence of c_f on $1/Ha$.

The extrapolation $Ha \to \infty$ allows us to compare c_f from our DNS and from the model of Lykoudis & Brouillette (1967) with the model of Alboussière & Lingwood (2000) in figure 5(*d*). The phenomenological model by Harris (1960) is also shown there. It assumes that the logarithmic layer is cut off by the plateau when the interaction parameter $N_\tau = Ha^2/Re_\tau$ based on Re_τ exceeds the threshold $N_\tau \approx 0.6$. Assuming that the plateau velocity equals the average velocity in the limit $Ha \to \infty$, formula (7.11) in Harris (1960) provides the relation

$$\sqrt{2/c_f} = 2.456 \ln\left(R^2 c_f/2\right) + 4.08, \tag{4.2}$$

plotted in figure 5(*d*). Since the velocity profiles of the previous section change from the logarithmic law to the plateau over a rather narrow z^+-interval and since, in addition, the agreement of our extrapolated DNS results with (4.2) is fairly good, a threshold criterion for N_τ may indeed apply for the non-overlap of the turbulent Hartmann layers (at least in the range of R values studied in the DNS). In contrast to the Harris model, the two mixing-length models overestimate our extrapolated DNS results for c_f.

5. Conclusions

Our systematic DNS study of turbulent Hartmann flow has focused on the dependence of mean flow properties on the parameters R and Ha. For fixed R we have examined how the case of an isolated turbulent Hartmann layer is approached upon increasing Ha. The mean velocity profile then develops a three-layer structure with an increasingly wide plateau. The logarithmic range broadens with R, and the coefficients of the logarithmic law approach those for ordinary hydrodynamic channel flow. This behaviour is in line with the argument from Alboussière & Lingwood (2000), who claim that MHD effects inside the Hartmann layer should be negligible because the local interaction parameter based on the laminar Hartmann layer thickness is small compared with unity. However, turbulent stress distributions from our DNS show a better agreement with the model of Lykoudis & Brouillette (1967), where additional MHD correction terms are incorporated in the mixing-length ansatz. It is tempting to interpret this as a low-Reynolds-number effect. The focus of future DNS should be on anisotropic features of the Joule dissipation and on statistical properties of the fluctuations in turbulent Hartmann flow.

We are grateful to Andre Thess, Yuri Kolesnikov and Oleg Zikanov for interesting discussions and useful comments, and to Bernard Knaepen, Daniele Carati and Stavros Kassinos, the organizers of the MHD Summer School 2005 at the Université Libre de Bruxelles, where this work was started. We also acknowledge financial support from the Deutsche Forschungsgemeinschaft. Computer resources were

https://doi.org/10.1017/S0022112006003673 Published online by Cambridge University Press

provided by the computing centers of TU Ilmenau and of the Forschungszentrum Jülich (NIC).

REFERENCES

Alboussière, T. & Lingwood, R. J. 2000 A model for the turbulent Hartmann layer. *Phys. Fluids* **12**, 1535–1543.

Branover, H. 1978 *Magnetohydrodynamic Flow in Ducts*. John Wiley.

Davidson, P. A. 1999 Magnetohydrodynamics in materials processing. *Annu. Rev. Fluid Mech.* **31**, 273–300.

Harris, L. P. 1960 *Hydromagnetic Channel Flows*. MIT Press and John Wiley.

Hartmann, J. 1937 Hg-dynamics I: Theory of the laminar flow of an electrically conductive liquid in a homogeneous magnetic field. *K. Dan. Vidensk. Selsk. Mat. Fys. Medd.* **15** (6), 1–28.

Hartmann, J. & Lazarus, F. 1937 Hg-dynamics II: Experimental investigations on the flow of mercury in a homogeneous magnetic field. *K. Dan. Vidensk. Selsk. Mat. Fys. Medd.* **15** (7), 1–45.

Kenjereš, S. & Hanjalić, K. 2000 On the implementation of effects of Lorentz force in turbulence closure models. *Intl J. Heat Fluid Flow* **21**, 329–337.

Knaepen, B., Kassinos, S. & Carati, D. 2004 Magnetohydrodynamic turbulence at moderate magnetic Reynolds number. *J. Fluid Mech.* **513**, 199–220.

Kobayashi, H. 2006 Large eddy simulation of magnetohydrodynamic turbulent channel flows with local subgrid-scale model based on coherent structures. *Phys. Fluids* **18**, 045107.

Krasnov, D. S., Zienicke, E., Zikanov, O., Boeck, T. & Thess, A. 2004 Numerical study of instability and transition to turbulence in the Hartmann flow. *J. Fluid Mech.* **504**, 183–211.

Lee, D. & Choi, H. 2001 Magnetohydrodynamic turbulent flow in a channel at low magnetic Reynolds number. *J. Fluid Mech.* **429**, 367–394.

Lykoudis, P. S. & Brouillette, E. C. 1967 Magneto-fluid-mechanic channel flow. ii. theory. *Phys. Fluids* **10**, 1002–1007.

Moreau, R. 2003 On turbulence in electromagnetic processing. In *Proc. 4th Intl Conf. on Electromagnetic Processing of Materials, 14–17 October, 2003, Lyon, France* (ed. S. Asai, Y. Fautrelle & P. Gillon).

Moresco, P. & Alboussière, T. 2004 Experimental study of the instability of the Hartmann layer. *J. Fluid Mech.* **504**, 167–181.

Moser, R. D., Kim, J. & Mansour, N. N. 1999 Direct numerical simulation of turbulent channel flow up to $Re_\tau = 590$. *Phys. Fluids* **11**, 943–945.

Satake, S., Kunugi, T., Naito, N., Takase, K. & Y., O. 2005 DNS of turbulent channel flow at high Reynolds number under a uniform magnetic field. In *15th Riga and 6th PAMIR Conference on Fundamental and Applied MHD* (ed. A. Alemany, A. Gailitis & G. Gerbeth), pp. 175–178. Riga, Latvia.

Widlund, O., Zahrai, S. & Bark, F. 1998 Development of a Reynolds stress closure for modelling of homogenous MHD turbulence. *Phys. Fluids* **10**, 1987.

Zienicke, E. A. & Krasnov, D. 2005 Parametric study of streak breakdown mechanism in Hartmann flow. *Phys. Fluids* **17**, 114101.

Zikanov, O. & Thess, A. 1998 Direct numerical simulation of forced MHD turbulence at low magnetic Reynolds number. *J. Fluid Mech.* **358**, 299–333.

https://doi.org/10.1017/S0022112006003673 Published online by Cambridge University Press